Journal of Marine Science and Technology, Vol. 23, No. 6, pp. 901-908 (2015)
DOI: 10.6119/JMST-015-0610-8

THEORETICAL ANALYSIS AND SPH SIMULATION FOR THE WAVE ENERGY CAPTURED BY A BOTTOM-HINGED OWSC

Yu-Chi Chang[1], Da-Wei Chen[2], Yi-Chih Chow[1], Shiaw-Yih Tzang[2]
Chen-Chou Lin[3], and Jiahn-Horng Chen[1]

Key words: Oscillating Wave Surge Converter (OWSC), power take-off (PTO), mechanical impedance, capture factor, Smoothed Particle Hydrodynamics (SPH).

ABSTRACT

This paper examines one type of wave energy converter, the Oscillating Wave Surge Converter (OWSC) with its bottom hinged on the sea bed. The simplest form of OWSC is a flapper connected with a power take-off (PTO). Theoretical analysis based on a 2D linear potential theory elucidates the mechanisms of the wave energy capture by a bottom-hinged OWSC in terms of impedances associated with the wave field, the flapper body, and the PTO. Criteria of impedance canceling and matching to maximize the energy capture factor can be deduced. Smoothed Particle Hydrodynamics (SPH) is established for simulating the same problem, and the trends of SPH results match that of the theoretical prediction well. Therefore, SPH can be regarded as a reliable numerical tool for designing and optimizing OWSCs.

I. INTRODUCTION

As the major portion of renewable energy from the ocean, wave energy has drawn significant attentions, resulting in many inventions and developments of wave energy converter (WEC). The European Marine Energy Center (EMEC) categorizes WECs into several types as follows (further information can be found at www.emec.org.uk): Attenuator, Point Absorber, Oscillating Wave Surge Converter (OWSC), Oscillating Water Column (OWC), Overtopping, Terminator, Submerged Pressure Differential, Bulge Wave, and Rotating Mass. For instance, the Pelamis (further information can be found at www.pelamiswave.com), which was the first commercialized WEC, pertains to the Attenuator type. The most popular, theoretically well-developed one among these WEC types is the Point Absorber, e.g., Falnes and Budal (1978), Evans (1981), Mei (1992), Falnes (2002). The most famous OWSC is the Oyster designed and manufactured by the UK company Aquamarine Power (further information can be found at www.aquamarinepower.com). Since the Oyster is a seabed-mounted, bottom-hinged flapper oscillating in the direction of wave surge (Folley et al., 2007; Whittaker and Folley, 2007), it is preferable to be installed at sites with water depth less than 40 meters, i.e., a near-shore or coastal application with significantly reduced complexities in engineering aspects. Bottom-hinged OWSCs like the Oyster have another advantage: their prime movers can be retracted toward the bottom to be fully submerged in the water in order to protect the whole device from huge waves during extreme weather conditions like typhoon or hurricane.

The OWSC can be regarded as a flapper (the prime mover) connected with a power take-off (PTO) system. The incident wave and the reflected and transmitted waves respectively brings in and take out from the device wave energy in the form of progressive wave. The residue enters the OWSC system and transforms into the kinetic energy (inertia) and the potential energy of gravity and buoyancy (restoring moment) of the flapper, and the kinetic energy (inertia), the potential energy (stiffness) and the take-off energy (damping) of the PTO. In this process, energy is transferred among different forms and adjusted by the presence of standing wave, resulting in mechanical impedances that interact among themselves to deeply affect the capture factor of the OWSC system (the ratio of the take-off energy to the incident wave energy). In order to develop a highly efficient OWSC, one needs to elucidate the mechanisms of how these impedances influence the wave energy capture by the device, and establish a reliable numerical scheme for simulating the hydrodynamic problem for

Paper submitted 12/16/14; revised 01/27/15; accepted 06/10/15. Author for correspondence: Yi-Chih Chow (e-mail: ycchow@mail.ntou.edu.tw).
[1] Department of System Engineering and Naval Architecture, National Taiwan Ocean University, Keelung, Taiwan, R.O.C.
[2] Department of Harbor and River Engineering, National Taiwan Ocean University, Keelung, Taiwan, R.O.C.
[3] Department of Mechanical and Mechatronic Engineering, National Taiwan Ocean University, Keelung, Taiwan, R.O.C.

design and optimization purposes.

This paper attempts to establish the Smoothed Particle Hydrodynamics (SPH) simulation for the wave energy capture of a bottom-hinged flapper. SPH is a mesh-free method and can be regarded as a Lagrangian technique originally developed for simulations of non-axisymmetric problems in astrophysics. This method was first proposed by Gingold and Monaghan (1977) and Lucy (1977) in late 1970s. Since then, many researchers have extended the application of SPH to many other fields including hydrodynamics with free surface (Monaghan, 1994), two-phase flows (Monaghan and Kocharyan, 1995), weakly incompressible flows (Morris, 1997; Morris and Monaghan, 1997), gravity flows (Monaghan, 1995), porous flows (Morris et al., 1999; Zhu et al., 1999; Shao, 2010), and so on, due to the fact that SPH has the capability of simulating moving objects with any shape. For more examples of applying SPH, Monaghan et al. (2003) simulated physical characteristics of the impact and entry of a rigid body traveling down a slope into water, and Gomez-Gesteira et al. (2010) simulated the movement of a caisson breakwater in the surf zone with a Riemann solver-based formulation, modeling the friction force between the moving caisson and the bed with a transition from static to dynamic friction force.

Previously, Chen et al. (2014) verified the wave-induced rotations of a bottom-hinged flapper without PTO using a modified SPHysics model (Gomez-Gesteira et al., 2012a; Gomez-Gesteira et al., 2012b) and found good agreements with experimental data. With that successful experience, this paper moves forward to simulate with SPH the energy-capturing performance of a bottom-hinged OWSC system (a flapper connected with a PTO), and compares the results of the simulation with that of the theoretical analysis based on the theory developed by Chang et al. (2014). In short, it is a 2D linear potential flow theory constructed to elucidate how the mechanical impedances associated with the flapper body and the PTO are combined with the impedances formed by the wave to affect the capture factor (details follow). Finally, conclusions about design strategies of the bottom-hinged OWSC and remarks on using SPH are given at the end of this paper.

II. 2D LINEAR POTENTAIL FLOW THEORY FOR BOTTOM-HINGED OWSC

1. 2D Boundary Problem

The following theoretical treatment and analysis for the 2D OWSC problem is adopted from Chang et al. (2014). The schematic of the 2D OWSC problem is illustrated in Fig. 1.

The left wave domain (Zone 1) consists of the incident wave (η_i), the reflected wave (η_r) from the flapper of the OWSC, and the standing wave (not shown) generated by the interaction between the flapper and the fluid. The right wave domain (Zone 2) consists of the progressive wave (η_p) generated by the motion of the flapper and the standing wave (not shown). The wave surges along the x-coordinate, and the

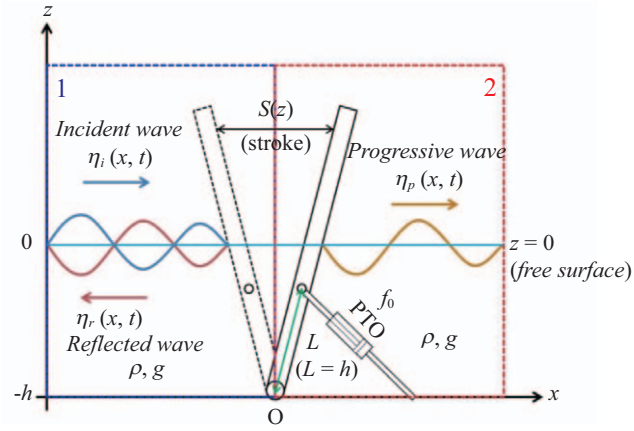

Fig. 1. Schematic of the 2D OWSC problem.

flapper is perpendicular to the still water surface ($z = 0$) and the seabed ($z = -h$) at $x = 0$, where h denotes the water depth. And ρ and g denote the water density and the acceleration of gravity, respectively. The hinge of the flapper is at the O point, and $S(z)$ means the horizontal stroke of the flapper that linearly varies with the water depth as follows:

$$S(z) = S_o(1+z^*) \tag{1}$$

where S_o means the maximum horizontal stroke of the flapper at $z = 0$, and $z^* = z/h$ denotes a non-dimensional water depth. The damping coefficient is denoted as f_o (unit: $\mathrm{kg/(s\cdot m)}$), and L (lever arm) is the distance between the joint of the PTO on the flapper and the hinge O. In order to simplify the problem, we assume that L is equal to h (water depth), which means that the joint of the PTO is regarded as connected to the top of the flapper. The real damping coefficient as used in the SPH simulation should be translated into the equivalent damping coefficient based on the assumption that $L = h$. We assume that the fluid is incompressible, inviscid, and irrotational, hence a velocity potential ϕ for the velocity filed that $\vec{u} = -\nabla\phi$ exists.

2. Moment-Balanced Equation

Incorporated with boundary conditions and appropriate linearizations, the moment-balanced equation for the 2D OWSC problem

$$M_w + M_{f_o} + M_M + M_{M_b} + M_{st} = \left(I + I_{PTO}\right)\cdot\ddot{\theta} \tag{2}$$

can be solved to show that

$$\left|S_o\right| = \frac{\frac{1}{\sigma h}\left(\left|A_i\right| G_p R_p\right)}{\sqrt{\left[W_1 + P_3\right]^2 + \left[W_2 + F_1 + F_2 + P_1 + P_2\right]^2}} \tag{3}$$

On the left-hand side of Eq. (2), M_w is the moment caused

by the difference of the fluid pressure on both sides of the flapper, M_{f_o} is the moment due to the PTO's damping force (assuming a constant damping coefficient f_o), M_M and M_{M_b} are moments due to the gravity and buoyancy forces, respectively, and M_{st} is the moment caused by the force due to the PTO's stiffness. On the right-hand side of Eq. (2), I and I_{PTO} are respectively the moments of inertia (per unit width) of the flapper and the PTO about the hinge O, and $\ddot{\theta}$ is the angular acceleration of the flapper. In Eq. (3), σ is the wave frequency, $|A_i|$ is the given amplitude of the velocity potential of the incident wave, and

$$W_1 = \frac{R_p^2 \cdot G_p}{k_i^*},\ W_2 = \sum_{n=1}^{\infty} \frac{R_s^2(n) \cdot G_s(n)}{k_s^*(n)} \tag{4}$$

$$F_1 = \frac{\left(m\overline{OM} - m_b\overline{OB}\right)g}{8\rho\sigma^2 h^4},\ F_2 = \frac{I\sigma^2}{8\rho\sigma^2 h^4} \tag{5}$$

$$P_1 = \frac{-Kh^2}{8\rho\sigma^2 h^4},\ P_2 = \frac{I_{PTO}\sigma^2}{8\rho\sigma^2 h^4},\ P_3 = f_o^* = \frac{f_o}{8\rho\sigma h^2} \tag{6}$$

$$G_p = \int_{-1}^{0} \cosh^2 k_i^*\left(1+z^*\right) dz^* \tag{7}$$

$$G_s(n) = \int_{-1}^{0} \cos^2\left[k_s^*(n)\left(1+z^*\right)\right] dz^* \tag{8}$$

$$R_p = \frac{\int_{-1}^{0} \frac{\left(1+z^*\right)}{2} \cosh k_i^*\left(1+z^*\right) dz^*}{\int_{-1}^{0} \cosh^2 k_i^*\left(1+z^*\right) dz^*} \tag{9}$$

$$R_s(n) = \frac{\int_{-1}^{0} \frac{\left(1+z^*\right)}{2} \cos\left[k_s^*(n)\left(1+z^*\right)\right] dz^*}{\int_{-1}^{0} \cos^2\left[k_s^*(n)\left(1+z^*\right)\right] dz^*} \tag{10}$$

where m and m_b denote respectively the masses (per unit width) of the flapper and its water displacement, $\overline{OM}$ and $\overline{OB}$ denote respectively the distances between the point O and the centers of mass and buoyancy, K denotes the stiffness (per unit width) of the PTO, and $k_i^* = k_i h$ and $k_s^*(n) = k_s(n)h$ are non-dimensional wave numbers of the incident wave and the standing wave, respectively.

3. Theoretical Capture Factor

In a wave period, the net work done to the PTO by the flapper reads

$$E_{f_0} = \int_0^{\frac{2\pi}{\sigma}} -M_{f_o}(t)\,\dot{\theta} dt = \frac{\pi}{4}\left(\sigma f_o\right)|S_o|^2 \tag{11}$$

where $\dot{\theta}$ is the angular velocity of the flapper. And the total incident wave energy in a wave period (E_i) is (Dean and Dalrymple, 1991)

$$E_i = \frac{\pi}{2}\rho|A_i|^2 \sinh 2k_i^* \left[\frac{1}{2}\left(\frac{2k_i^*}{\sinh k_i^*}\right)\right] \tag{12}$$

Finally, the theoretical capture factor (CF) of OWSC is derived

$$CF = \frac{E_{f_0}}{E_i} = \frac{2\left(W_1 \cdot P_3\right)}{\left(W_1 + P_3\right)^2 + \left(W_2 + F_1 + F_2 + P_1 + P_2\right)^2} \tag{13}$$

where every term on the right-hand side of Eq. (13) can be regarded as a form of mechanical impedance. According to their natures, these terms can be named as: W_1 as the progressive-wave impedance, W_2 as the standing-wave impedance, F_1 as the flapper-restoring-moment impedance (can also be interpreted as the hydrostatic stiffness of the flapper), F_2 as the flapper-inertia impedance, P_1 as the PTO-stiffness impedance, P_2 as the PTO-inertia impedance, and P_3 as the PTO-damping impedance, i.e., the dimensionless damping coefficient of PTO.

According to Eq. (13), it can be shown that the capture factor reaches its maximum value of 0.5 when $W_2 + F_1 + F_2 + P_1 + P_2 = 0$, i.e., the sum of the impedances related to the stiffness and the inertia of the flapper and the PTO cancels the impedance due to the standing wave generated (the criterion of impedance canceling) and $W_1 = P_3$, i.e., the impedances related to the PTO's damping matches the impedance due to the progressive waves generated (the criterion of impedance matching). In practical situations, the effects of P_1 and P_2 are much smaller than that of other impedances. Therefore, the criterion of impedance cancelling stated above can be reasonably rewritten as $W_2 + F_1 + F_2 = 0$. The impedances W_2 and F_2 can be shown to be always positive (Eqs. (4, 5, 8)). Therefore, $W_2 + F_1 + F_2 = 0$ requires F_1 to be negative. In other words, the moment $\left(m\overline{OM} - m_b\overline{OB}\right)g$ should be negative (Eq. (5)), i.e., the so-called "restoring moment."

III. SPH METHOD

1. Governing Equation

The governing equations of SPH are based on the Navier-Stokes equations, consisting of the continuity and the momentum equations describing the motion of a viscous flow. The equations are expressed as follows:

$$\frac{d\rho}{dt} = \sum_{b=1}^{N} m_b \vec{u}_{ab} \cdot \nabla_a W_{ab} \tag{14}$$

$$\frac{d\vec{u}_a}{dt} = \sum_{b=1}^{N} m_b \left(\frac{P_a}{\rho_a^2} + \frac{P_b}{\rho_b^2}\right) \cdot \nabla_a W_{ab} + \Pi_{ab} + \vec{g} \tag{15}$$

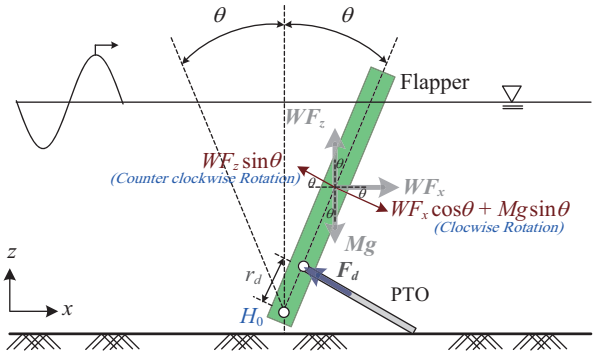

Fig. 2. Definition sketch of the bottom-hinged flapper.

where $\vec{u}_{ab} = \vec{u}_a - \vec{u}_b$ is the velocity of the particle, W_{ab} the kernel function, m the mass of each particle, P the pressure, $\vec{g}$ the gravitational acceleration, ρ the fluid particle density, υ the fluid viscosity and and $\prod_{ab}$ an empirical approximation of the viscosity effects by Monaghan (1994).

2. Numerical Scheme

According to Monaghan (1994), the force on each boundary particle is computed by summing up the contribution from all the surrounding water particles. Denoting the force per unit mass on a moving body boundary particle k by f_k, the equation is given by

$$f_{wp} = M\frac{dV}{dt} = \sum_k m_k f_k \tag{16}$$

where M is the mass of a rigid body, V is the velocity of the center of mass, subscript wp denotes water particle, and f_{wp} is the force per unit mass exerted by the water particle on the boundary particle.

In Fig. 2, the total toque for rotations of a flapper from the wave-induced torque and the torque by body force and the reversed damping torque can be written as

$$\tau_t = \tau_w + \tau_b - \tau_d \tag{17}$$

in which

$$\tau_w = \left(WF_x \cdot \cos\theta - WF_z \cdot \sin\theta\right) \times r_{H_0}$$

$$= \left(\sum f_{wp\_x} \cdot \cos\theta - \sum f_{wp\_z} \cdot \sin\theta\right) \times r_{H_0} \tag{18}$$

$$\tau_b = Mg \cdot \sin\theta \times r_{H_0} = \sum\left(m_{bp} \cdot g\right) \cdot \sin\theta \times r_{H_0} \tag{19}$$

$$\tau_d = r_d \times F_d \tag{20}$$

where r_{H_0} is the distance from each boundary particle to the hinge at H_0. The WF_x and WF_z are the total forces by waves in horizontal (f_{wp_x}) and vertical (f_{wp_z}) directions, respectively. The symbol g denotes the gravitational acceleration. F_d is the damping force relating to the tangential velocity on the connecting position between the flapper and damping to control the flapper motion and absorb wave energy. The total torque must be larger than the revised damping torque and then the flapper could be driven to rotate.

From total torque τ_t, the angular acceleration of the rotating flapper $d\omega/dt$ can be found by

$$\frac{d\omega}{dt} = \frac{\tau_t}{I} \tag{21}$$

where I and ω denote the moment of inertia and the angular velocity, respectively.

For the rotating flapper, the angular velocity $d\theta/dt$ can be obtained by the angular acceleration $d\omega/dt$ in the last time step. Hence, the instantaneous angular velocity can be obtained as

$$\left(\frac{d\theta}{dt}\right)^{n+1} = \left(\frac{d\theta}{dt}\right)^{n} + \left(\frac{d\omega}{dt}\right)^{n} \cdot \Delta t \tag{22}$$

where superscript "n+1 " denotes the computed value in the next time step with Δt being the time step using quasi-linear assumption.

3. Wave Energy Capture

In order to further understand the wave energy captured by the flapper and transferred through the PTO during an average wave cycle, the captured energy (E_{f0}) of a flapper can be calculated using

$$E_{f0} = \int_0^T \tau_d(t)\omega(t)dt \tag{23}$$

where T denotes the wave period or rotating period of the flapper. Hence, the simulated capture factor (CF) of OWSC with the total incident wave energy (E_i) and the captured energy (E_{f0}) in a wave period can be expressed as

$$CF = \frac{E_{f_0}}{E_i} \tag{24}$$

4. Numerical Setups for Simulation

For considering high computational efficiency and high resolutions in simulation, the previously adopted 2-D SPH numerical wave flume is slightly shortened with a length of 13 m and a water depth of 0.5 m. A piston-type wave-maker is set on the upstream and a 1:5 slope on the downstream boundaries for reducing reflected waves, as shown in Fig. 3. The simulations adopt a particle spacing of dx = dz = 0.02 m, and the empirical coefficient α of 0.05 for the artificial viscosity term.

Table 1. The incident waves and simulation conditions.

ID		T (s)	H (cm)	f_0 (kg/s/m)	$P_3 = f_0^*$	Density (kg/m^3)
Case A	1	1.57	7.7	780.4	0.0039	555
	2			2361.20	0.0118	555
	3			5242.66	0.0262	555
	4			13686.94	0.0684	555
	5			26353.36	0.1317	555
	6			35838.17	0.1791	555
	7			2361.20	0.0118	1000
	8			2361.20	0.0118	7000
	9			26873.62	0.1343	7000
	10			65733.32	0.3285	7000
Case B	1	1.33	7.6	755.87	0.0032	555
	2			2314.86	0.0098	555
	3			5173.00	0.0219	555
	4			13487.59	0.0571	555
	5			25959.48	0.1099	555
	6			35313.39	0.1495	555
	7			2314.86	0.0098	1000
	8			2314.86	0.0098	7000
	9			28881.54	0.1083	7000
	10			65052.23	0.2754	7000
Case C	1	1.11	7.4	735.87	0.0026	555
	2			2235.91	0.0079	555
	3			4952.96	0.0175	555
	4			12906.00	0.0456	555
	5			24849.71	0.0878	555
	6			33793.55	0.1194	555
	7			2235.91	0.0079	1000
	8			2235.91	0.0079	7000
	9			24255.36	0.0857	7000
	10			60595.94	0.2141	7000

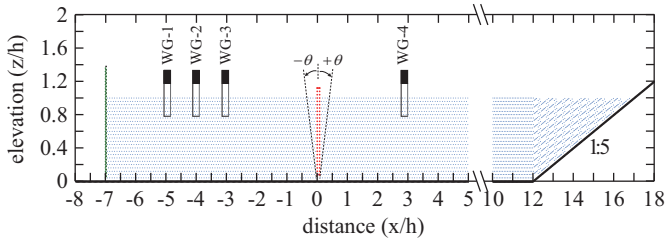

Fig. 3. Model setups and normalized coordinate system from Chen et al. (2014)

In addition, all the parameters used in the theoretical analysis as listed in Table 1 are adopted for calculating corresponding capture factors and flapping angles.

IV. RESULTS

1. Theoretical Analysis

Following the consideration of Chang et al. (2014) and corresponding to the SPH simulation performed in this paper,

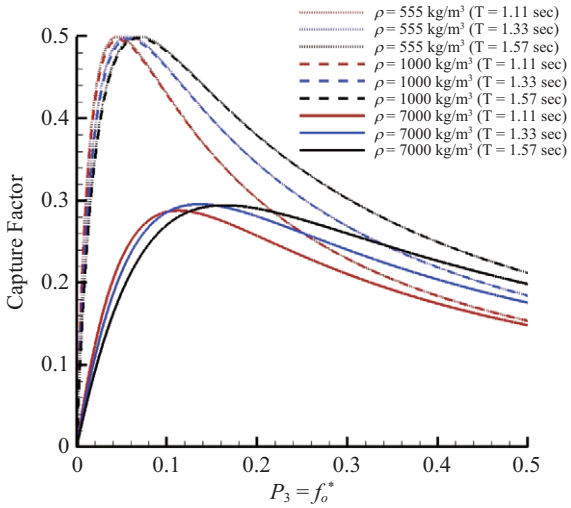

Fig. 4. Variations of theoretical capture factor with the PTO-damping impedance (P_3) or the dimensionless damping coefficient of PTO for cases of three periods of incoming wave (T = 1.11, 1.33, 1.57 sec) and three densities of the flapper body (ρ = 555, 1000, 7000 kg/m^3).

three periods of incoming wave, T = 1.11, 1.33, 1.57 sec, are chosen to be used in computing the theoretical capture factor (*CF*) with Eq. (13) and other equations related to mechanical impedances. Fig. 4 presents the variations of the theoretical *CF* with the PTO-damping impedance or the dimensionless damping coefficient of PTO at these three cases of wave period and three cases of density of the flapper body, ρ = 555, 1000, 7000 kg/m^3, corresponding to three regimes of specific gravity: smaller than 1, equal to 1, and greater than 1, respectively. All the curves in Fig. 4 show a similar pattern: a much steeper slope of the curve on the left of the peak than that on the right. It implies that the variation of the *CF* on the left of the peak is much more sensitive to the change of the PTO's damping than that on the right, resulting in different damping-control strategies to approach the maximum *CF*.

For the case of ρ = 555 kg/m^3, the optimum PTO-damping impedance (denoted as P_3^{opt}) at which the peak of *CF* resides increases with the wave period, resulting in opposite quantity orders of *CF* on different sides of the peaks, i.e., $CF(T_1, P_3) > CF(T_2, P_3)$ if $T_1 < T_2$ when $P_3 < P_3^{opt}$; $CF(T_1, P_3) < CF(T_2, P_3)$ if $T_1 < T_2$ when $P_3 > P_3^{opt}$. The peak values of *CF* for all wave periods for the case of ρ = 555 kg/m^3 are very close to 0.5 (i.e. the maximum theoretical value of *CF*), indicating that the criterion of impedance matching dominates the criterion of impedance canceling, i.e., $(W_1 + P_3)^2 \gg (W_2 + F_1 + F_2 + P_1 + P_2)^2$ in the denominator of Eq. (13). This result may imply that more attentions need to be paid to the damping control of PTO as long as the specific gravity of the flapper body is smaller than 1. For the case of ρ = 1000 kg/m^3, it is clearly evident in Fig. 4 that the curves are almost identical to that for the case of ρ = 555 kg/m^3. Therefore, the description and analysis for the

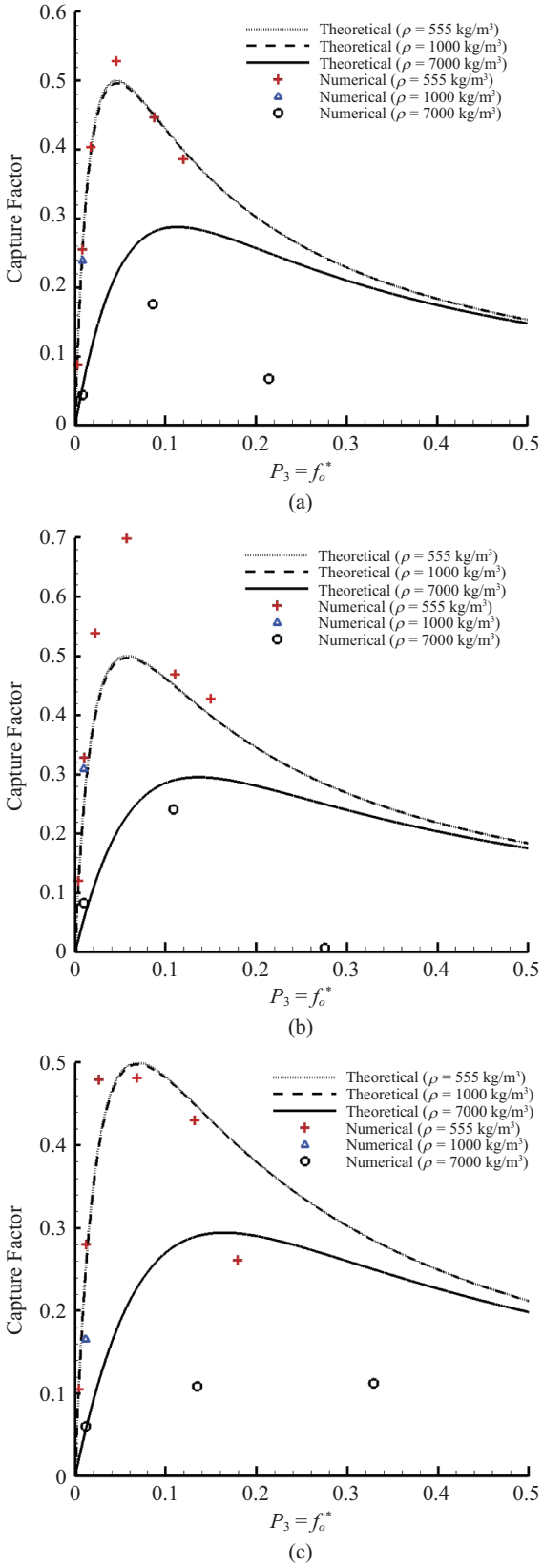

Fig. 5. Comparisons of capture factor between theoretical and SPH results for cases of three densities of the flapper body (ρ = 555, 1000, 7000 kg/m^3) at wave periods of (a) T = 1.11 sec, (b) T = 1.33 sec, and (c) T = 1.57 sec.

case of ρ = 555 kg/m^3 presented above applies as well here.

For the case of ρ = 7000 kg/m^3, which can be exemplified as a solid flapper body of iron, significant reductions of the peak values of *CF* from 0.5 can be observed, meaning that the departure from the criterion of impedance canceling is so large such that it is now comparable to the criterion of impedance matching, i.e., $(W_1 + P_3)^2 \approx (W_2 + F_1 + F_2 + P_1 + P_2)^2$ in the denominator of Eq. (13). Still, the optimum PTO-damping impedance in this case increases with the wave period.

2. SPH Simulation

Based on the characteristics of the performance curves shown in Fig. 4 and described in the theoretical analysis presented above, three values of P_3 smaller than P_3^{opt}, P_3^{opt} itself, and two values of P_3 greater than P_3^{opt} are chosen to be used in the SPH simulation for the case of ρ = 555 kg/m^3. In addition, one value and three values of P_3 are chosen for the cases of ρ = 1000 and 7000 kg/m^3, respectively. As shown in Fig. 5(a), the simulated *CF*s at T = 1.11 sec for the cases of ρ = 555 and 1000 kg/m^3 match the theoretical curves pretty well, except for the point at P_3^{opt} with a little more departure from the theoretical value. For the cases of ρ = 555 and 1000 kg/m^3 at T = 1.33 sec as shown in Fig. 5(b), however, the simulated *CF*s of the third and the forth points at P_3 smaller than and equal to P_3^{opt}, respectively, are significantly greater than the corresponding theoretical values. The reason behind this departure is not clear to us now. Nevertheless, we conjecture that wave reflections from the boundaries of the simulation domain and their interactions with the incident wave to possibly form some sort of standing wave may play a role in this disparity between theoretical and SPH results. For the cases of ρ = 555 and 1000 kg/m^3 at T = 1.57 sec as shown in Fig. 5(c), the simulated *CF*s seem to be back on track with the theoretical curves except for the last point. Over all, it should suffice to say that the theoretical trends of the capture factor for the cases of ρ = 555 and 1000 kg/m^3, e.g., P_3^{opt}, are well simulated by SPH.

For the case of ρ = 7000 kg/m^3 as shown in Fig. 5, the simulated *CF*s are not able to catch the theoretical trends, as so are the simulated flapping angles as shown in Fig. 6, with even totally opposite trend as shown in Fig. 6(c). Nevertheless, the simulated flapping angles match the theoretical curves relatively well for the cases of ρ = 555 and 1000 kg/m^3 as shown in Fig. 6. These results seem to suggest that appropriate weight designations to the particles representing the flapper body according to the body density are quite important. In the future, we will investigate whether making the weights of particles of the fluid and the flapper body closer to each other increases the accuracy of the simulation.

V. CONCLUSION

Theoretical analysis and SPH simulation are performed to

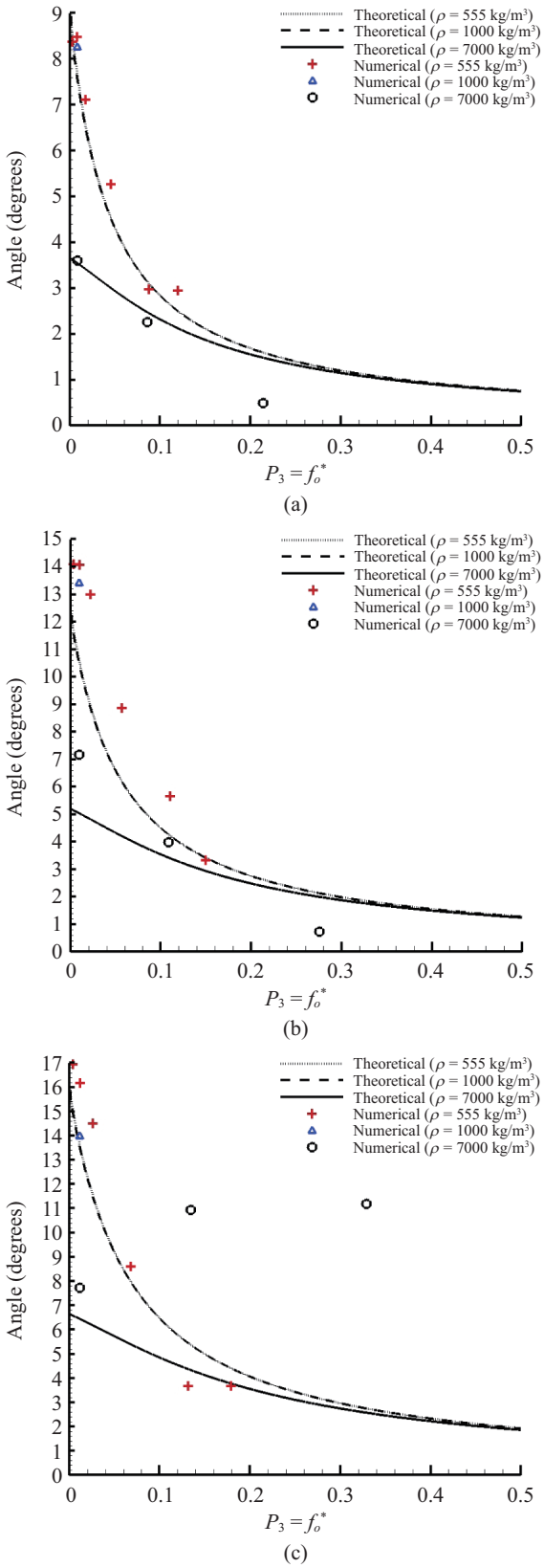

Fig. 6. Comparisons of flapping angle between theoretical and SPH results for cases of three densities of the flapper body (ρ = 555, 1000, 7000 kg/m^3) at wave periods of (a) T = 1.11 sec, (b) T = 1.33 sec, and (c) T = 1.57 sec.

investigate the problem of the wave energy captured by a bottom-hinged OWSC. In terms of impedances associated with the wave field, the flapper body, and the PTO, a 2D linear potential flow theory elucidates that the maximum capture factor can be reached when the sum of the impedances related to the stiffness and the inertia of the flapper and the PTO cancels the impedance due to the standing wave generated and the impedances related to the PTO's damping matches the impedance due to the progressive waves generated. These theoretical results and trends not only indicate control and design strategies for the bottom-hinged OWSC, but also provide verification and validation to the SPH simulation. SPH results match the theoretical trends well for the cases of ρ = 555 and 1000 kg/m^3, but not for the case of ρ = 7000 kg/m^3. Further improvements on reducing the wave reflections from the boundaries of the simulation domain and making the weight of the flapper body particles as close to that of the fluid particles as possible may be the key to better accuracy of the SPH simulation. Over all, SPH can be used as a reliable numerical tool for designing and optimizing OWSCs.

ACKNOWLEDGMENTS

This work was financially supported by the Ministry of Science and Technology of Taiwan (formerly the National Science Council of Taiwan). The grant numbers are NSC100-3113-E-019-001-, NSC100-2221-E-019-066-, and NSC101-3113-E-019-002-.

REFERENCES

Chang, Y. C., Y. H. Lee, Y. C. Chow, C. C. Lin, S. Y. Tzang and J. H. Chen (2014). Mechanical impedance effects on the capture factor of OWSC. Journal of Taiwan Society of Naval Architects and Marine Engineers 33, 183-192. (in Chinese)

Chen, D. W., S. Y. Tzang, C. M. Hsieh, Y. C. Chow, J. H. Chen, C. C. Lin and R. R Hwang (2014). Numerical modeling of wave-induced rotations of a bottom-hinged flapper with a SPH model. Journal of Marine Science Technology – Taiwan 22, 372-380.

Dean, R. G. and R. A. Dalrymple (1991). Water Wave Mechanics for Engineers and Scientists. World Scientific.

Evans, D. V. (1981). Power from Water Waves. Annual Review of Fluid Mechanics 13, 157-187.

Falnes, J. (2002). Ocean Waves and Oscillating Systems. Cambridge University Press.

Falnes, J. and K. Budal (1978). Wave-power conversion by point absorbers. Norwegian Maritime Research 6, 2-11.

Folley, M., T. Whittaker and J. Van't Hoff (2007). The design of small seabed-mounted bottom-hinged wave energy converters. Proceedings of the 7th European Wave and Tidal Energy Conference, Porto, Portugal.

Gingold, R. A. and J. J. Monaghan (1977). Smoothed particle hydrodynamics - Theory and application to non-spherical stars. Monthly Notices of the Royal Astronomical Society 181, 375-389.

Gomez-Gesteira, M., A. J. C. Crespo, B. D. Rogers, R. A. Dalrymple, J. M. Dominguez and A. Barreiro (2012a). SPHysics – development of a free-surface fluid solver – Part 2: Efficiency and test cases. Computers & Geosciences 48, 300-307.

Gomez-Gesteira, M., B. D. Rogers, A. J. C. Crespo, R. A. Dalrymple, M. Narayanaswamy and J. M. Dominguez (2012b). SPHysics – development of a free-surface fluid solver – Part 1: Theory and formulations. Com-

puters & Geosciences 48, 289-299.
Gomez-Gesteira, M., B. D. Rogers, R. A. Dalrymple and A. J. C. Crespo (2010). State-of-the-art of classical SPH for free-surface flows. Journal of Hydraulic Research 48, 6-27.
Lucy, L. B. (1977). Numerical approach to the testing of the fission hypothesis. Astronomical Journal 82, 1013-1024.
Mei, C. C. (1992). The Applied Dynamics of Ocean Surface Waves. World Scientific.
Monaghan, J. J. (1994). Simulating free surface flows with SPH. Journal of Computational Physics 110, 399-406.
Monaghan, J. J. (1995). Simulating gravity currents with SPH lock gates. Mathematics Reports and Preprints 95.
Monaghan, J. J. and A. Kocharyan (1995). SPH simulation of multi-phase flow. Computer Physics Communications 87, 225-235.
Monaghan, J. J., A. Kos and N. Issa (2003). Fluid motion generated by impact. Journal of Waterway Port Coastal and Ocean Engineering-Asce 129, 250-259.
Morris, J. (1997). Modeling low Reynolds number incompressible flows using SPH. Journal of Computational Physics 136, 214-226.
Morris, J. P. and J. J. Monaghan (1997). A switch to reduce SPH viscosity. Journal of Computational Physics 136, 41-50.
Morris, J. P., Y. Zhu and P. J. Fox (1999). Parallel simulations of pore-scale flow through porous media. Computers and Geotechnics 25, 227-246.
Shao, S. D. (2010). Incompressible SPH flow model for wave interactions with porous media. Coastal Engineering 57, 304-316.
Whittaker, T. and M. Folley (2007). The Oyster wave energy converter. Proceedings of the 7th European Wave and Tidal Energy Conference, Portugal.
Zhu, Y., P. J. Fox and J. P. Morris (1999). A pore-scale numerical model for flow through porous media. International Journal for Numerical and Analytical Methods in Geomechanics 23, 881-904.